Cancer Science
The official journal of the Japanese Cancer Association

Evaluation of [^{125}I]IPOS as a molecular imaging probe for hypoxia-inducible factor-1-active regions in a tumor: Comparison among single-photon emission computed tomography/X-ray computed tomography imaging, autoradiography, and immunohistochemistry

Masashi Ueda,[1,2] Takashi Kudo,[2] Yasuko Mutou,[3] Izumi Ogihara Umeda,[3] Azusa Miyano,[2] Kei Ogawa,[2] Masahiro Ono,[2] Hirofumi Fujii,[3] Shinae Kizaka-Kondoh,[4] Masahiro Hiraoka[5] and Hideo Saji[2,6]

[1]Radioisotopes Research Laboratory, Kyoto University Hospital, Faculty of Medicine, Kyoto University, Kyoto; [2]Department of Patho-Functional Bioanalysis, Graduate School of Pharmaceutical Sciences, Kyoto University, Kyoto; [3]Functional Imaging Division, Research Center for Innovative Oncology, National Cancer Center Hospital East, Kashiwa; [4]Department of Biomolecular Engineering, Graduate School of Bioscience and Biotechnology, Tokyo Institute of Technology, Yokohama; [5]Department of Radiation Oncology and Image-Applied Therapy, Graduate School of Medicine, Kyoto University, Kyoto, Japan

(Received March 10, 2011/Revised July 26, 2011/Accepted August 2, 2011/Accepted manuscript online August 8, 2011/Article first published online September 15, 2011)

To image hypoxia-inducible factor-1 (HIF-1)-active tumors, we previously developed a chimeric protein probe ([$^{123/125}$I]IPOS) that is degraded in the same manner as HIF-1α under normoxic conditions. In the present study, we aim to show that the accumulation of radioiodinated POS reflects the expression of HIF-1. *In vivo* single-photon emission computed tomography (SPECT)/X-ray CT (CT) imaging, autoradiography, and double-fluorescent immunostaining for HIF-1α and pimonidazole (PIMO) were carried out 24 h after the injection of [^{125}I]IPOS. Tumor metabolite analysis was also carried out. A tumor was clearly visualized by multi-pinhole, high-resolution SPECT/CT imaging with [^{125}I]IPOS. The obtained images were in accordance with the corresponding autoradiograms and with the results of *ex vivo* biodistribution. A metabolite analysis revealed that 77% of the radioactivity was eluted in the macromolecular fraction, suggesting that the radioactivity mainly existed as [^{125}I]IPOS in the tumors. Immunohistochemistry revealed that the HIF-1α-positive areas and PIMO-positive areas were not always identical, only some of the regions were positive for both markers. The areas showing [^{125}I]IPOS accumulation were positively and significantly correlated with the HIF-1α-positive areas ($R = 0.75$, $P < 0.0001$). The correlation coefficient between [^{125}I]IPOS-accumulated areas and HIF-1α-positive areas was significantly greater than that between the [^{125}I]IPOS-accumulated areas and the PIMO-positive areas ($P < 0.01$). These findings indicate that [^{125}I]IPOS accumulation reflects HIF-1 expression. Thus, [$^{123/125}$I]IPOS can serve as a useful probe for the molecular imaging of HIF-1-active tumors. (*Cancer Sci* 2011; 102: 2090–2096)

The expansion of a tumor mass implies the development of cancer cells that are distant from blood vessels. Cells outgrow their vascular supply, leading to the lowering of oxygen partial pressure below physiologic levels (i.e., hypoxia). Hypoxia-inducible factor-1 (HIF-1) is a key transcriptional regulator in response to hypoxia.[1] Overexpression of HIF-1 has been indicated in over 70% of human cancers (e.g. breast, prostate, brain, lung, head and neck cancers) and their metastases compared to that of adjacent normal tissue.[2] Clinical studies associate the hypoxic status of a tumor with bad prognosis and resistance to chemotherapy and radiotherapy.[3] Furthermore, several HIF-1 inhibitors have been developed to inhibit tumor growth and to overcome resistance to therapies.[4] Thus, non-invasive imaging of HIF-1-active regions in a tumor provides useful information for qualitative cancer diagnosis, cancer therapy, and improving the effectiveness of HIF-1 inhibitors.

The expression of HIF-1 in tumors has been shown to be affected by the microenvironment in each tumor, resulting in heterogeneous HIF-1 tumor activity and expression.[5] Moreover, HIF-1 has been reported to be expressed even in a small tumor spheroid (<1 mm in diameter).[6] Therefore, a high spatial resolution device was required for the accurate imaging of HIF-1-expressed regions. Several techniques to improve spatial resolution, such as depth-of-interaction scintillators, image reconstruction using time-of-flight information, and multi-pinhole collimators, have recently been developed[7–10] and incorporated into commercially available PET and single-photon emission computed tomography (SPECT) systems. These modalities enable the detailed visualization of intratumoral HIF-1 expression in both animal models and humans.

Hypoxia-inducible factor-1 is composed of two subunits, HIF-1α and HIF-1β. The former is rapidly degraded by the ubiquitin–proteasome pathway under normoxic conditions, but it is stabilized under hypoxic conditions and regulates HIF-1 transcriptional activity. The proteasomal degradation of HIF-1α occurs through protein hydroxylation on proline residues in the oxygen-dependent degradation domain (ODD) of HIF-1α.[11,12] Thus, it is expected that probes containing the ODD and that are degraded in manner similar to HIF-1α can evaluate HIF-1 activity *in vivo*.

Based on the above concept, we recently developed a protein in which the protein transduction domain (PTD)[13] and a monomeric streptavidin (SAV) are fused to the ODD. We also synthesized a radiolabeled biotin derivative, (3-[$^{123/125}$I]iodobenzoyl)norbiotinamide ([$^{123/125}$I]IBB) and conjugated the chimeric protein, PTD-ODD-SAV (POS), and [$^{123/125}$I]IBB to produce [$^{123/125}$I]IBB-POS ([$^{123/125}$I]IPOS). POS was degraded in an oxygen-dependent manner, and a clear tumor image was obtained by planar imaging at 24 h after the injection of [^{123}I]IPOS. The intratumoral distribution of [^{125}I]IPOS corresponded to the hypoxic

[6]To whom correspondence should be addressed.
E-mail: hsaji@pharm.kyoto-u.ac.jp

doi: 10.1111/j.1349-7006.2011.02057.x

areas. However, direct comparison between the area showing [^{125}I]IPOS accumulation and HIF-1α expression was not carried out in the previous study.[14] Moreover, the 3D distribution of HIF-1-active regions in tumors has not been extensively evaluated *in vivo*. We then compared [^{125}I]IPOS distribution to HIF-1 expression by autoradiographic and immunohistochemical studies in the present study. Moreover, we attempted to image the detailed intratumoral distribution of [^{125}I]IPOS, which potentially reflects the heterogeneous expression of HIF-1, using a multi-pinhole, high-resolution small animal SPECT. The purpose of the present study is to reveal whether [$^{123/125}$I]IPOS can be used to visualize HIF-1-active regions in a tumor.

Materials and Methods

Animal model. Animal studies were carried out in accordance with our institutional guidelines, and the experimental procedures were approved by the Kyoto University Animal Care Committee (Kyoto, Japan) and the Ethical Committee for Animal Experiments of the National Cancer Center (Kashiwa, Japan). Five-week-old female C3H/He mice were purchased from Japan SLC (Hamamatsu, Japan) and kept at a constant ambient temperature under a 12-h light/dark cycle with free access to food and water. FM3A mouse mammary carcinoma cells were cultured and s.c. implanted in the right thigh as described in previous reports.[14,15] Approximately 2 weeks after the implantation, the mice were subjected to a tracer study. The average diameter of the tumors was 10 mm.

Radiosynthesis of [^{125}I]IPOS. POS was overexpressed in *Escherichia coli* and purified, as described in a previous report.[14] Purified POS was dissolved in Tris–HCl buffer (pH 8.0).

Sodium [^{125}I]iodide was purchased from PerkinElmer Life and Analytical Sciences (Boston, MA, USA). As described in a previous report,[14] [^{125}I]IBB was synthesized with a radiochemical yield of 40–50%. [^{125}I]IPOS was synthesized by incubation of [^{125}I]IBB and POS for 1 h followed by purification using Sephadex G50 columns (GE Healthcare Bioscience, Uppsala, Sweden). Using [^{125}I]IBB as a starting material, [^{125}I]IPOS was obtained with a radiochemical yield of >85% and a radiochemical purity of >95%.

***In vivo* and *ex vivo* SPECT/CT imaging.** Two FM3A-bearing mice were used in this study. They were i.v. injected with [^{125}I]IPOS (30 μg, 23 MBq), and 24 h later, CT and SPECT images were acquired under 1.5% isoflurane anesthesia. A SPECT/CT combined scanner was used to acquire sectional images; the scanner had four detectors equipped with tungsten-based, multiplexing multi-pinhole collimators dedicated for small animal imaging (NanoSPECT/CT; Bioscan, Washington, DC, USA).

First, CT scans were carried out under the following conditions: tube voltage, 45 kV; tube current, 177 μA; and tube current-time product (the product of tube current and scan time), 32 mAs. The obtained CT data were reconstructed using a cone-beam filtered back-projection method with InVivoScope (Bioscan) postprocessing software.

The SPECT scans were then carried out. In the SPECT system, each collimator had nine pinholes, each with a diameter of 1.4 mm and a cylindric field of view of 32 mm in diameter × 16 mm in length. The axial field of view was extended using a step-and-shoot helical SPECT with a user-defined range of up to 230 mm, based on the region to be imaged. The energy peak for the camera was set to 28 keV, and the energy window was set to peak energy ± 30%, that is, 20–36 keV. *In vivo* SPECT acquisition was carried out in six steps over 90° (300 s per step), with four detectors covering 360°. The total acquisition time to scan a range of 71.9 mm was 90 min per mouse. The acquired SPECT data were reconstructed with HiSPECT postprocessing software (SciVis, Göettingen, Germany) by an ordered subsets–expectation maximization algorithm designed for multiplexing multi-pinhole reconstruction.

Both SPECT and CT images were automatically coregistered because both systems shared the same axis of rotation, allowing for the combination of scintigraphic and anatomic information in all tomographic scans in three different spatial axes.

After *in vivo* imaging, the mice were killed and the tumors were carefully excised. The *ex vivo* SPECT image of each tumor was acquired for 60 min with an acquisition time of 600 s per projection. The tumors were then frozen and cut into 6-μm-thick sections for H&E staining and into 20-μm-thick sections for autoradiography. The sections were prepared in the same direction of the SPECT slice. The section corresponding to the SPECT image was selected according to the slice thickness and used for autoradiography.

***Ex vivo* biodistribution, autoradiography, and immunohistochemistry.** FM3A-bearing mice ($n = 5$) were i.v. injected with [^{125}I]IPOS (30 μg, 3.2 MBq); 22 h later, they were i.p. injected with pimonidazole (PIMO; 60 mg/kg). After another 2 h, the mice were killed. Whole organ specimens were immediately removed, weighed, and their radioactivity was measured with an auto-well gamma counter (Wizard 1480; PerkinElmer, Waltham, MA, USA). The results were expressed in terms of the percent injected dose per gram of tissue (%ID/g). The tumors were removed and divided into two parts. The radioactivity of one part was counted, and the other part was immediately frozen. After freezing, 10-μm-thick sections of tumor were prepared with a cryomicrotome (CM1900; Leica Microsystems, Wetzlar, Germany). Two sections were prepared from each tumor, and autoradiograms of these sections were obtained, according to a previously described method,[16,17] but with the following minor modification: a BAS5000 scanner was used instead of a BAS3000 scanner (both scanners; Fuji Photo Film, Tokyo, Japan). The same slides used in the autoradiographic study were subjected to dual fluorescent immunostaining for HIF-1α and PIMO.[15,18] Adjacent sections on each autoradiogram were stained with H&E to identify the necrotic regions.

Size-exclusion analysis of radioactive compounds in tumors. After an i.v. injection of [^{125}I]IPOS (30 μg, 4.4 MBq), FM3A-bearing mice ($n = 3$) were housed in metabolic cages (Metabolica; Sugiyama-Gen, Tokyo, Japan) for 24 h for the collection of urine and feces. Subsequently, the mice were killed. Extracts from the tumors and the feces were prepared by using a previously reported method,[15,18,19] with slight modifications. In brief, the tumors and feces were homogenized, and the preparations were centrifuged at 5000g at 4°C for 30 min. The supernatants and urine were analyzed by size-exclusion chromatography (PD-10; GE Healthcare Bioscience). In addition, aliquots of the supernatants from the tumors were analyzed by size-exclusion high-performance liquid chromatography (HPLC; TSKgel SuperSW2000; 4.6 × 300 mm; Tosoh, Tokyo, Japan) (100 mM phosphate buffer [pH 6.8], 0.2 mL/min).

Image analyses of autoradiograms and immunohistochemical images. Ten square regions of interest (ROIs) were selected from the viable regions that showed [^{125}I]IPOS accumulation on each autoradiogram and were then transferred to the corresponding immunohistochemical image. The positions of the ROIs in both images were confirmed on the basis of the x- and y-positions of each ROI that were displayed in both the softwares. The quantification of radioactivity in each ROI and the determination of the levels of HIF-1α expression and PIMO-adduct formation were carried out according to the previously reported method.[15]

Statistical analyses. Correlation coefficients were assessed using Spearman's rank analysis. A chi-square-test was used to compare the correlation coefficients between [^{125}I]IPOS-accumulated areas and HIF-1α- or PIMO-positive areas. Values of $P < 0.05$ were considered statistically significant.

Results

***In vivo* and *ex vivo* SPECT/CT imaging.** Representative SPECT/CT images are shown in Figure 1. The images indicate a clear and specific accumulation of radioactivity in the FM3A tumor at 24 h after [^{125}I]IPOS injection. Compared to the tumor, there was no [^{125}I]IPOS accumulation in the opposite leg (Fig. 1A,B,D). The serial axial images documented that the intratumoral distribution pattern of [^{125}I]IPOS was heterogeneous (Fig. 1E). The bladder can be seen in rostral-side slices.

Figure 2 shows *ex vivo* SPECT images and corresponding autoradiograms. Although autoradiograms showed intratumoral distribution of [^{125}I]IPOS in more detail due to its higher spatial resolution than SPECT images, a similar distribution pattern of [^{125}I]IPOS was observed in both images. Staining with H&E depicted necrotic regions in the tumor (Fig. 2, N), without the accumulation of [^{125}I]IPOS.

***Ex vivo* biodistribution.** Table 1 shows the biodistribution of [^{125}I]IPOS in FM3A xenografts at 24 h after injection. A high level of radioactivity was found to be accumulated in the liver and intestine, and a moderate level was present in the kidneys and tumor, and a low level was present in the muscle and neck. The tumor accumulation was 1.7%ID/g, the tumor/blood ratio was 5.6, and the tumor/muscle ratio was 10. These results were consistent with those of a previous report.[14]

Size-exclusion analysis of radioactive compounds in tumors. The recovery of radioactivity from tumor homogenates was 83% (SD, 3.8%). In the analysis using PD-10, most of the radioactive material was eluted in macromolecular fractions (77% [10%]). Moreover, by size-exclusion HPLC analysis, radioactivity was detected at approximately 34 kDa, which is

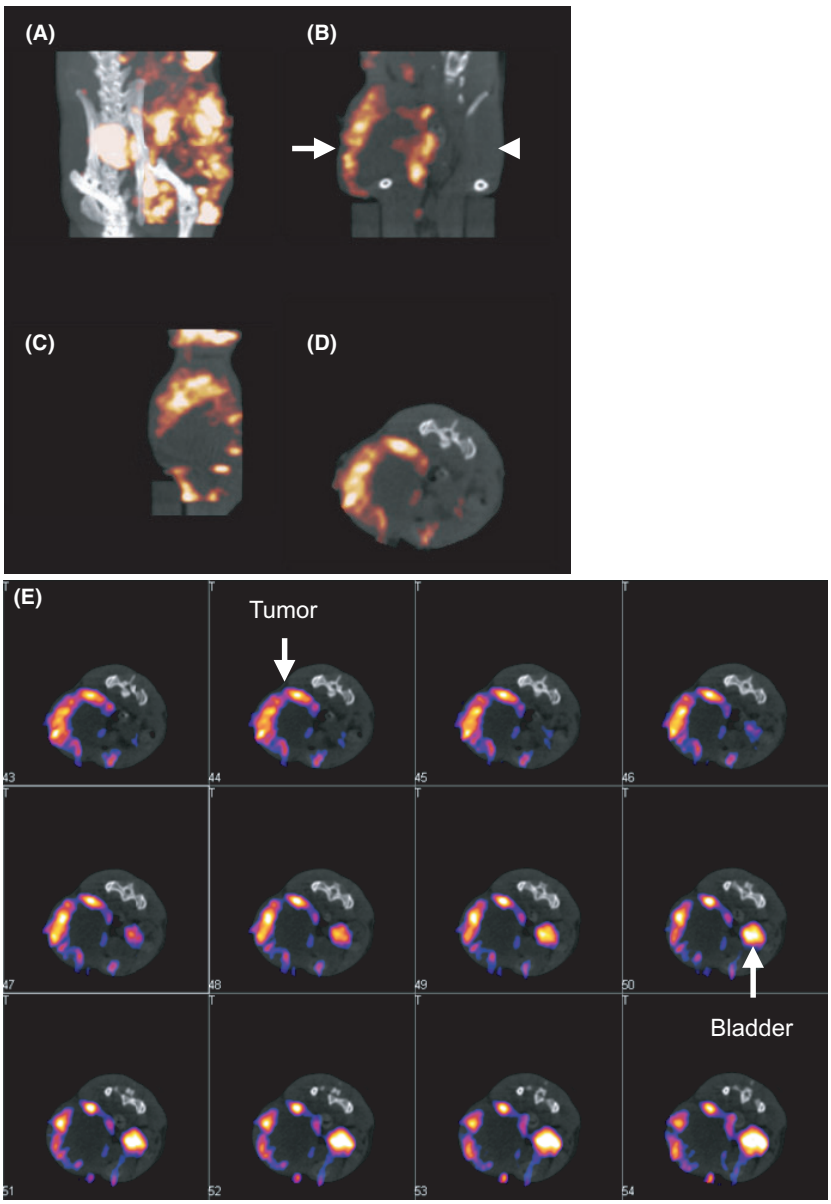

Fig. 1. Representative single-photon emission computed tomography/computed tomography fusion images of FM3A-bearing mouse obtained 24 h after injection of [^{125}I]IPOS. Maximum intensity projection (A), coronal (B), sagittal (C), and axial (D) images are shown. The arrow indicates the tumor in the right thigh, and the arrowhead indicates the corresponding area in the opposite leg in (B). Serial axial images (slice thickness, 0.3 mm) are also shown in (E).

doi: 10.1111/j.1349-7006.2011.02057.x

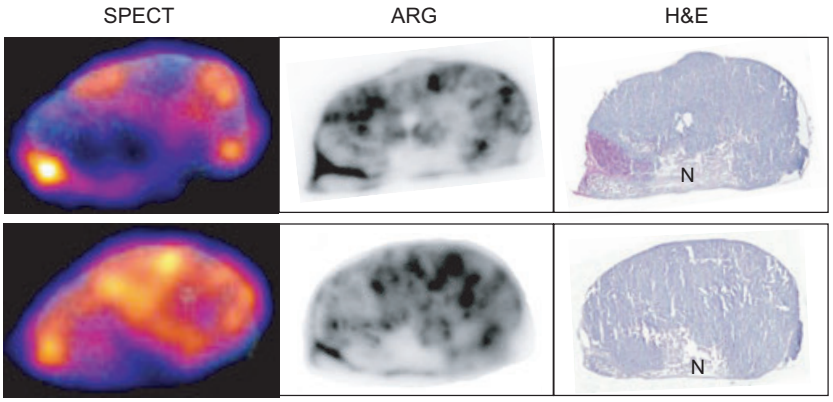

Fig. 2. *Ex vivo* single-photon emission computed tomography (SPECT) images with corresponding autoradiograms (ARG) and H&E stained sections. The images were obtained 25.5 h after injection of [^{125}I]IPOS. N, necrotic region.

Table 1. Biodistribution of [^{125}I]IPOS at 24 h in FM3A-xenografted mice (%ID/g)

Tissue	Radioactivity
Blood	0.31 ± 0.03
Liver	15.93 ± 1.11
Intestine	6.34 ± 1.55
Kidneys	3.40 ± 1.54
Tumor	1.71 ± 0.26
Muscle	0.18 ± 0.04
Neck†	0.10 ± 0.02
Urine†‡	45.85 ± 7.30
Feces†‡	26.27 ± 10.71
Tumor/blood ratio	5.57 ± 1.01
Tumor/muscle ratio	10.09 ± 2.82

Values are mean ± SD; $n = 5$. †Expressed as %ID. ‡$n = 3$.

the molecular weight of POS. In contrast, the radioactive material in feces homogenates and urine was rarely eluted in macromolecular fractions (5.6% [3.0%] and 0.36% [0.06%], respectively).

Autoradiography and immunohistochemistry. The autoradiogram represented that the distribution of [^{125}I]IPOS in the tumor was heterogeneous (Fig. 3A). Dual fluorescent immunohistochemistry indicated the presence of HIF-1α- and PIMO-positive hypoxic areas in the tumors (Fig. 3B,C). High-magnification merged imaging of HIF-1α and PIMO immunostaining revealed the presence of PIMO-positive areas along the edge of the HIF-1α-positive areas. However, HIF-1α-positive areas and PIMO-positive areas were not always identical. Some regions were positive for both, whereas other regions did not overlap (Fig. 3D). The majority of [^{125}I]IPOS-accumulated areas corresponded to the HIF-1α-positive areas (Fig. 3A,B).

We then compared correlations between [^{125}I]IPOS accumulation and HIF-1α or PIMO expression levels. As shown in Figure 4, areas with [^{125}I]IPOS accumulation showed a positive correlation with both HIF-1α- and PIMO-positive areas (HIF-1α: $R = 0.75$, $P < 0.0001$; PIMO: $R = 0.48$, $P = 0.0002$). The correlation coefficient between [^{125}I]IPOS and HIF-1α was significantly greater than that with PIMO ($\chi^2 = 8.38$, $P < 0.01$).

Discussion

A number of hypoxia imaging probes, such as [^{18}F]fluoromisonidazole ([^{18}F]FMISO), 1-α-D-(5-deoxy-5-[^{18}F]fluoroarabinofuranosyl)-2-nitroimidazole ([^{18}F]FAZA), and [$^{60/64}$Cu]Cu-diacetyl-bis(N^4-methylthiosemicarbazone) ([$^{60/64}$Cu]Cu-ATSM), have been developed and used in clinical studies.[20,21] These probes detect physically low oxygen partial pressure (<10 mmHg) and are useful for predicting the efficacy of radiotherapy.[22] In fact, clinical PET studies with [^{60}Cu]Cu-ATSM have shown an inverse relationship between the tumor uptake of [^{60}Cu]Cu-ATSM and the response to therapy in patients with lung and rectal carcinomas.[21] However, the mechanisms underlying hypoxic accumulation of these probes are not dependent on HIF-1 expression and further studies are necessary to decisively determine the role of them in identifying HIF-1-active regions in tumors.

The expression level of HIF-1α was reported to increase dramatically as the oxygen partial pressure decreased below 40 mmHg.[23] Furthermore, it was reported that the oxygen concentrations at which HIF-1 activity occurs differ among tissue cells.[3,23] For example, pulmonary cells are consistently exposed to relatively high oxygen concentrations, and thus, the oxygen concentrations that these cells perceive as abnormal are relatively high. However, bone marrow cells, which usually exist under low oxygen concentrations, require no HIF-1 activity when they are kept under the same oxygen concentrations as pulmonary cells.[5] Therefore, probes that detect absolute physical oxygen partial pressures are not enough when attempting to detect the expression or activity of HIF-1. Because HIF-1 is associated with tumor progression, angiogenesis, metastasis, and resistance to chemo- and radiotherapy, HIF-1 imaging would provide significant information for characterizing tumor phenotype and would be useful for predicting prognosis. Thus, multiple details on tumor characterization, treatment strategy, and prognosis would be provided by linking [^{123}I]IPOS-SPECT with [^{18}F]FMISO-, [^{18}F]FAZA-, or [$^{60/64}$Cu]Cu-ATSM-PET.

Recently, nuclear medical imaging[24–26] and bioluminescent imaging[27,28] based on HIF-1-responsive reporter systems have been successfully carried out. However, these systems required exogenous gene transfection. To surmount this limitation, our research group developed a number of injectable protein probes, including [^{125}I]IPOS, which contain ODD and degrade in an oxygen-dependent manner. These probes have been used successfully to visualize hypoxic tumors on planar nuclear medical imaging[14,15] and optical imaging.[1,5,29] However, the *in vivo* 3D distribution of HIF-1-active regions in tumors has not been extensively evaluated in our previous studies. Thus, we were challenged to obtain high spatial resolution tomographic images using multi-pinhole SPECT. Multi-pinhole SPECT systems have recently provided greatly improved efficiency with high spatial resolution and have overcome the resolution versus sensitivity trade-off.[30] The disadvantage of SPECT is a quantitative

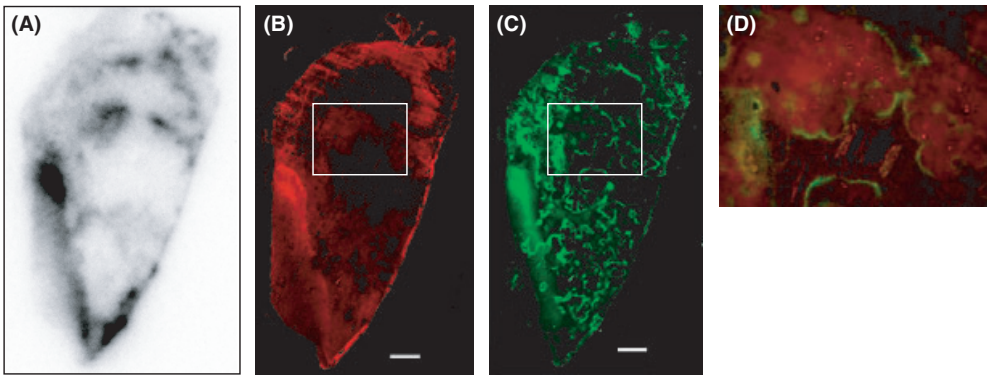

Fig. 3. Representative images of an autoradiogram (A), hypoxia-inducible factor (HIF)-1α immunostaining (B), and pimonidazole immunostaining (C) in the identical section. A high-magnification merged image of HIF-1α immunostaining with pimonidazole immunostaining (D, from insets in B,C) shows that some regions were positive for both stains (yellow) but others did not overlap (red or green). Bars = 1 mm (B,C).

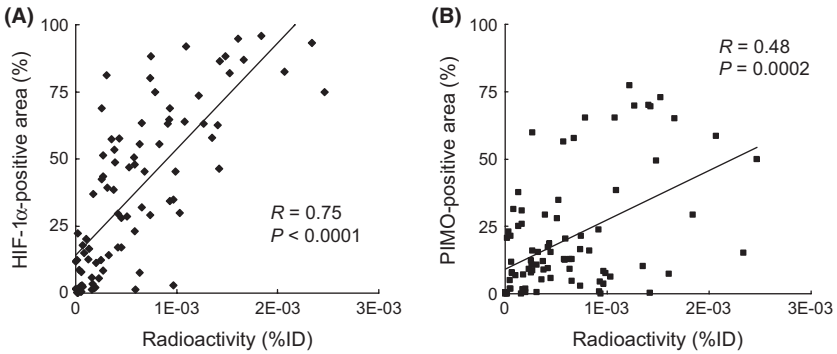

Fig. 4. Correlation between the intratumoral distribution of [^{125}I]IPOS and the level of hypoxia-inducible factor (HIF)-1α expression (A) or that of pimonidazole (PIMO)-adduct formation (B). The ordinate represents the percentage of HIF-1α- and PIMO-positive areas in each region of interest (ROI), and the abscissa represents [^{125}I]IPOS accumulation (%ID) in the same ROI. A total of 10 sections (two sections per tumor) were analyzed. Regression analysis of the areas showing [^{125}I]IPOS accumulation with HIF-1α- or PIMO-positive areas reveal a significantly positive correlation in both cases (HIF-1α: $R = 0.75$, $P < 0.0001$; PIMO: $R = 0.48$, $P = 0.0002$). The results of the chi-square-test reveal that the correlation coefficient between [^{125}I]IPOS and HIF-1α was significantly higher than that between [^{125}I]IPOS and PIMO ($P < 0.01$).

performance due to difficulties in attenuation and scattering correction, and the sensitivity of multi-pinhole SPECT is still lower than PET. However, because SPECT can theoretically achieve a higher spatial resolution than PET, wherein the resolution is limited by the positron range, it is suitable for small animal imaging. In fact, several multi-pinhole SPECT systems are able to image small components within mouse organs.[31,32] The *in vivo* images obtained in the present study were consistent with the results of *ex vivo* biodistribution. The tumor was clearly visualized, but no accumulation of radioactivity was observed in the opposite leg (Fig. 1A,B,D), indicating a high tumor/muscle ratio (10 in *ex vivo* biodistribution). Our observation of high radioactivity in the bladder (Fig. 1E) was in accordance with the finding that the radioactivity was mainly excreted in urine after the administration of [^{125}I]IPOS.

The characterization of [^{125}I]IPOS has been reported in a previous study.[14] Although the tumor uptake of [^{125}I]IPOS was significantly and positively correlated with HIF-1 transcriptional activity, suggesting the feasibility of [^{125}I]IPOS as an HIF-1-active tumor imaging probe, a direct comparison between the intratumoral distribution of [^{125}I]IPOS and HIF-1 expression has not yet been carried out. In the present study, the majority of the [^{125}I]IPOS-distributed areas in the tumor corresponded to HIF-1α-positive hypoxic areas, although there were a few unmatched regions (Fig. 3). A significant positive correlation was observed between the areas, and the correlation coefficient between [^{125}I]IPOS and HIF-1α was significantly greater than that between [^{125}I]IPOS and PIMO (Fig. 4). Although we cannot exclude the effect of the difference in the molecular sizes of [^{125}I]IPOS and PIMO on the distribution, these findings are consistent with the results of recent studies showing that HIF-1α-positive areas are not always colocalized with PIMO-positive areas.[33–35] Thus, [^{125}I]IPOS can be viewed as a probe that depicts HIF-1-active areas rather than the physically hypoxic areas themselves.

Although the detailed mechanism of cellular uptake and retention of [^{125}I]IPOS is now under investigation, we found that low temperature (4°C) or ATP depletion inhibited the cellular uptake of [^{125}I]IPOS (unpublished data). As most studies have shown endocytosis as the major cellular uptake pathway for most PTDs[36,37] and endocytosis occurs in an energy-dependent manner, [^{125}I]IPOS is probably uptaken by the cells through the endocytotic pathway. After uptake by endocytosis, [^{125}I]IPOS could be released from the endosomes and retained intracellularly because of its molecular size. In fact, in our previous experiment, [^{125}I]IPOS was not cleared from the cells under hypoxic conditions for at least 24 h, after the incubation medium was replaced with fresh medium.[14] Although the intracellular radioactivity decreased gradually under normoxic conditions, the cleared radioactivity was mainly attributable to the small molecules.[14] These findings indicated the intracellular retention ability of [^{125}I]IPOS.

doi: 10.1111/j.1349-7006.2011.02057.x

In the present study, the biodistribution of [^{125}I]IPOS was consistent with a previous report;[14] thus, the reproducibility of the biodistribution of [^{125}I]IPOS was confirmed. Although the amount of tumoral accumulation of [^{125}I]IPOS was not as high as that of 2-[^{18}F]fluoro-2-deoxy-D-glucose ([^{18}F]FDG), this could have been due to the limited expression of HIF-1. The expression of HIF-1 is not ubiquitous, but heterogeneous, and is small in tumors.[6] In fact, the probe accumulation in the tumors harboring HIF-1-dependent reporter genes was 1–2%ID/g in previous studies,[6,38,39] which is comparable to the results of the present study. The size-exclusion analysis revealed that the radioactivity in the tumor existed as 34-kDa macromolecules that were most likely [^{125}I]IPOS existing stably in hypoxic regions. Furthermore, the radioactivity in urine and feces were mainly in low-molecular-weight compounds. This was consistent with our previous *in vitro* findings showing that [^{125}I]IPOS was degraded in normoxic cells and that [^{125}I]IBB and other small molecules were cleared from the cells.[14] Thus, these findings prove the concept of [^{125}I]IPOS *in vivo* and show that [^{125}I]IPOS exists stably only in the HIF-1-active regions while undergoing degradation and clearance in normoxic regions.

Although HIF-1α was reported to degrade within a few minutes under normoxic conditions,[5] the degradation of [^{125}I]IPOS was relatively slow.[14] Thus, a long exposure time is necessary to obtain sufficiently contrasting images; this is one of the drawbacks of [^{125}I]IPOS. Moreover, a study has shown that the acute hypoxic region created by the shutdown of blood vessels can be reoxygenated after reopening the blood vessels.[40] In such reoxygenated areas especially, the inconsistency in the rates of degradation of HIF-1α and [^{125}I]IPOS may be responsible for the differences in the distribution pattern of [^{125}I]IPOS and HIF-1α expression. POS comprises not only the ODD, which is the essential domain related to oxygen-dependent degradation, but also the PTD and SAV. This modification may hamper the degradation of the probe. However, this is not a substantial problem; a pretargeting approach can overcome this drawback. In fact, a 4–8-fold earlier visualization of the tumor can be achieved with the SAV–radiolabeled biotin-based pretargeting approach.[15,18]

In conclusion, multi-pinhole high-resolution SPECT/CT imaging with [^{125}I]IPOS clearly visualized a tumor. The obtained images were in accordance with the corresponding autoradiograms and the analysis of *ex vivo* biodistribution. The autoradiograms documented that the intratumoral distribution of [^{125}I]IPOS was heterogeneous and showed a good correlation with HIF-1α-positive areas. These findings indicate that the distribution of [^{125}I]IPOS reflects the expression of HIF-1α, thus rendering [$^{123/125}$I]IPOS an effective probe for the molecular imaging of HIF-1-active tumors.

Acknowledgments

This work was supported in part by ''R&D of Molecular Imaging Equipment for Malignant Tumor Therapy Support'' by the New Energy and Industrial Technology Development Organization, Japan, a Health Labour Sciences Research Grant for Research on Advanced Medical Technology from the Ministry of Health, Labour and Welfare of Japan, and a Grant-in-Aid for Exploratory Research (17659010) and a Grant-in-Aid for Young Scientists (B) (21791187) from the Ministry of Education, Culture, Sports, Science and Technology of Japan.

Disclosure Statement

The authors have no conflict of interest.

References

1 Kizaka-Kondoh S, Konse-Nagasawa H. Significance of nitroimidazole compounds and hypoxia-inducible factor-1 for imaging tumor hypoxia. *Cancer Sci* 2009; **100**: 1366–73.
2 Zhong H, De Marzo AM, Laughner E *et al.* Overexpression of hypoxia-inducible factor 1alpha in common human cancers and their metastases. *Cancer Res* 1999; **59**: 5830–5.
3 Semenza GL. Targeting HIF-1 for cancer therapy. *Nat Rev Cancer* 2003; **3**: 721–32.
4 Schwartz DL, Powis G, Thitai-Kumar A *et al.* The selective hypoxia inducible factor-1 inhibitor PX-478 provides in vivo radiosensitization through tumor stromal effects. *Mol Cancer Ther* 2009; **8**: 947–58.
5 Kizaka-Kondoh S, Tanaka S, Harada H, Hiraoka M. The HIF-1-active microenvironment: an environmental target for cancer therapy. *Adv Drug Deliv Rev* 2009; **61**: 623–32.
6 Serganova I, Doubrovin M, Vider J *et al.* Molecular imaging of temporal dynamics and spatial heterogeneity of hypoxia-inducible factor-1 signal transduction activity in tumors in living mice. *Cancer Res* 2004; **64**: 6101–8.
7 Lecomte R. Novel detector technology for clinical PET. *Eur J Nucl Med Mol Imaging* 2009; **36** (Suppl 1): S69–85.
8 Lewellen TK. Recent developments in PET detector technology. *Phys Med Biol* 2008; **53**: R287–317.
9 Riemann B, Schafers KP, Schober O, Schafers M. Small animal PET in preclinical studies: opportunities and challenges. *Q J Nucl Med Mol Imaging* 2008; **52**: 215–21.
10 Rowland DJ, Cherry SR. Small-animal preclinical nuclear medicine instrumentation and methodology. *Semin Nucl Med* 2008; **38**: 209–22.
11 Wang GL, Jiang BH, Rue EA, Semenza GL. Hypoxia-inducible factor 1 is a basic-helix-loop-helix-PAS heterodimer regulated by cellular O_2 tension. *Proc Natl Acad Sci USA* 1995; **92**: 5510–4.
12 Choi HJ, Song BJ, Gong YD, Gwak WJ, Soh Y. Rapid degradation of hypoxia-inducible factor-1alpha by KRH102053, a new activator of prolyl hydroxylase 2. *Br J Pharmacol* 2008; **154**: 114–25.
13 Kizaka-Kondoh S, Itasaka S, Zeng L *et al.* Selective killing of hypoxia-inducible factor-1-active cells improves survival in a mouse model of invasive and metastatic pancreatic cancer. *Clin Cancer Res* 2009; **15**: 3433–41.
14 Kudo T, Ueda M, Kuge Y *et al.* Imaging of HIF-1-active tumor hypoxia using a protein effectively delivered to and specifically stabilized in HIF-1-active tumor cells. *J Nucl Med* 2009; **50**: 942–9.
15 Ueda M, Kudo T, Kuge Y *et al.* Rapid detection of hypoxia-inducible factor-1-active tumours: pretargeted imaging with a protein degrading in a mechanism similar to hypoxia-inducible factor-1alpha. *Eur J Nucl Med Mol Imaging* 2010; **37**: 1566–74.
16 Ueda M, Iida Y, Tominaga A *et al.* Nicotinic acetylcholine receptors expressed in the ventralposterolateral thalamic nucleus play an important role in anti-allodynic effects. *Br J Pharmacol* 2010; **159**: 1201–10.
17 Temma T, Ogawa Y, Kuge Y *et al.* Tissue factor detection for selectively discriminating unstable plaques in an atherosclerotic rabbit model. *J Nucl Med* 2010; **51**: 1979–86.
18 Kudo T, Ueda M, Konishi H *et al.* PET imaging of hypoxia-inducible factor-1-active tumor cells with pretargeted oxygen-dependent degradable streptavidin and a novel (18)F-labeled biotin derivative. *Mol Imaging Biol* 2010; 10.1007/s11307-010-0418-6 [Epub ahead of print].
19 Motta-Hennessy C, Sharkey RM, Goldenberg DM. Metabolism of indium-111-labeled murine monoclonal antibody in tumor and normal tissue of the athymic mouse. *J Nucl Med* 1990; **31**: 1510–9.
20 Postema EJ, McEwan AJ, Riauka TA *et al.* Initial results of hypoxia imaging using 1-alpha-D-(5-deoxy-5-[^{18}F]-fluoroarabinofuranosyl)-2-nitroimidazole (^{18}F-FAZA). *Eur J Nucl Med Mol Imaging* 2009; **36**: 1565–73.
21 Dunphy MP, Lewis JS. Radiopharmaceuticals in preclinical and clinical development for monitoring of therapy with PET. *J Nucl Med* 2009; **50** (Suppl 1): 106S–21S.
22 Krohn KA, Link JM, Mason RP. Molecular imaging of hypoxia. *J Nucl Med* 2008; **49** (Suppl 2): 129S–48S.
23 Jiang BH, Semenza GL, Bauer C, Marti HH. Hypoxia-inducible factor 1 levels vary exponentially over a physiologically relevant range of O_2 tension. *Am J Physiol* 1996; **271**: C1172–80.
24 Yeom CJ, Chung JK, Kang JH *et al.* Visualization of hypoxia-inducible factor-1 transcriptional activation in C6 glioma using luciferase and sodium iodide symporter genes. *J Nucl Med* 2008; **49**: 1489–97.
25 He F, Deng X, Wen B *et al.* Noninvasive molecular imaging of hypoxia in human xenografts: comparing hypoxia-induced gene expression with endogenous and exogenous hypoxia markers. *Cancer Res* 2008; **68**: 8597–606.

26 Carlin S, Pugachev A, Sun X *et al.* In vivo characterization of a reporter gene system for imaging hypoxia-induced gene expression. *Nucl Med Biol* 2009; **36**: 821–31.
27 Harada H, Kizaka-Kondoh S, Itasaka S *et al.* The combination of hypoxia-response enhancers and an oxygen-dependent proteolytic motif enables real-time imaging of absolute HIF-1 activity in tumor xenografts. *Biochem Biophys Res Commun* 2007; **360**: 791–6.
28 Moroz E, Carlin S, Dyomina K *et al.* Real-time imaging of HIF-1alpha stabilization and degradation. *PLoS One* 2009; **4**: e5077.
29 Kuchimaru T, Kadonosono T, Tanaka S, Ushiki T, Hiraoka M, Kizaka-Kondoh S. In vivo imaging of HIF-active tumors by an oxygen-dependent degradation protein probe with an interchangeable labeling system. *PLoS One* 2010; **5**: e15736.
30 Grassi R, Cavaliere C, Cozzolino S *et al.* Small animal imaging facility: new perspectives for the radiologist. *Radiol Med* 2009; **114**: 152–67.
31 Pissarek M, Meyer-Kirchrath J, Hohlfeld T *et al.* Targeting murine heart and brain: visualisation conditions for multi-pinhole SPECT with (99m)Tc- and (123)I-labelled probes. *Eur J Nucl Med Mol Imaging* 2009; **36**: 1495–509.
32 van der Have F, Vastenhouw B, Ramakers RM *et al.* U-SPECT-II: an ultra-high-resolution device for molecular small-animal imaging. *J Nucl Med* 2009; **50**: 599–605.
33 Lehmann S, Stiehl DP, Honer M *et al.* Longitudinal and multimodal in vivo imaging of tumor hypoxia and its downstream molecular events. *Proc Natl Acad Sci U S A* 2009; **106**: 14004–9.
34 Li XF, Carlin S, Urano M, Russell J, Ling CC, O'Donoghue JA. Visualization of hypoxia in microscopic tumors by immunofluorescent microscopy. *Cancer Res* 2007; **67**: 7646–53.
35 Sobhanifar S, Aquino-Parsons C, Stanbridge EJ, Olive P. Reduced expression of hypoxia-inducible factor-1alpha in perinecrotic regions of solid tumors. *Cancer Res* 2005; **65**: 7259–66.
36 Madani F, Lindberg S, Langel U, Futaki S, Graslund A. Mechanisms of cellular uptake of cell-penetrating peptides. *J Biophys* 2011; **2011**: 414729.
37 Nakase I, Takeuchi T, Tanaka G, Futaki S. Methodological and cellular aspects that govern the internalization mechanisms of arginine-rich cell-penetrating peptides. *Adv Drug Deliv Rev* 2008; **60**: 598–607.
38 Hsieh CH, Kuo JW, Lee YJ, Chang CW, Gelovani JG, Liu RS. Construction of mutant TKGFP for real-time imaging of temporal dynamics of HIF-1 signal transduction activity mediated by hypoxia and reoxygenation in tumors in living mice. *J Nucl Med* 2009; **50**: 2049–57.
39 Wen B, Burgman P, Zanzonico P *et al.* A preclinical model for noninvasive imaging of hypoxia-induced gene expression; comparison with an exogenous marker of tumor hypoxia. *Eur J Nucl Med Mol Imaging* 2004; **31**: 1530–8.
40 Kizaka-Kondoh S, Inoue M, Harada H, Hiraoka M. Tumor hypoxia: a target for selective cancer therapy. *Cancer Sci* 2003; **94**: 1021–8.

doi: 10.1111/j.1349-7006.2011.02057.x